Materials Chemistry and Physics 311 (2024) 128576

Contents lists available at ScienceDirect

Materials Chemistry and Physics

journal homepage: www.elsevier.com/locate/matchemphys

Room-temperature SnO_2-based sensor with Pd-nanoparticles for real-time detection of CO dissolved gas in transformer oil

Agnes Nascimento Simões [a], Glauco Meireles Mascarenhas Morandi Lustosa [b], Eugênio de Souza Morita [a,b], André Nunes de Souza [c], Floriano Torres [d], Waldir Antonio Bizzo [a], Talita Mazon [b,*]

[a] Universidade de Campinas, Faculdade de Engenharia Mecânica, Campinas/SP, Brazil
[b] Centro de tecnologia da Informação Renato Archer, Campinas/SP, Brazil
[c] Universidade Estadual de São Paulo, Departamento de Engenharia Elétrica, Bauru/SP, Brazil
[d] HOG, CPFL Geração, Campinas/SP, Brazil

HIGHLIGHTS

- Synthesis of SnO_2 nanostructures decorated with Pd-Nanoparticles.
- Development of immersed sensor board for power transformers.
- CO detection sensitivity less than 20 ppm dissolved into oil at room temperature.
- Efficiency for real-time monitoring through *in situ* electrical measurements.
- Potential industrial applications for failure prevention of equipment and hazards.

ARTICLE INFO

Keywords:
Tin dioxide
Gas sensor
Carbon monoxide
Dissolved gas analysis
Transformer oil

ABSTRACT

SnO_2 and Pd nanoparticles (NPs) were synthesized by hydrothermal method and sol-gel, respectively. A paste formed by tin dioxide NP and PVDF was deposited as thick film on alumina substrates through screen printing method and decorated with Pd on surface. The morphology and structure of the samples were investigated by Scanning Electronic Microscopy (SEM), X-Ray Diffraction (XRD) and Raman Spectroscopy. The SEM images show SnO_2 nanoparticles with rod shapes and 10–15 nm of diameter size and Pd spherical nanograins with 15–35 nm of diameter. XRD analysis identifies rutile structure for SnO_2 powder and cubic structure for Pd NP. To investigate the gas sensing property of the SnO_2:Pd nanostructured composite, the electrodes were immersed in an insulating mineral oil, in a closed system where different gas concentration of monoxide carbon (CO) were injected into the headspace and then dissolved into oil, according to Ostwald coefficient. All measurements were carried out at room temperature using a concentration range from 50 to 500 ppm (in headspace). The electric characterization showed that our SnO_2-based sensor had change its resistance in a lower concentration of dissolved gas, ~13.3 ppm of CO, into the mineral oil, indicating its potential use for real time monitoring of transformers.

1. Introduction

In high voltage power systems, the power transformer is considered the most critical and high-value equipment, an important device that operates with insulation oil and has cooling functions on both transmission and distribution power grid systems. Some unavoidable insulation defects in a long-life transformer may arise [such as overheat (pyrolysis), partial discharge (corona) and insulation degradation] and then generate some gases [carbon oxides (CO, CO_2), hydrogen (H_2) and hydrocarbons (CH_4, C_2H_4, C_2H_2)] that can be present dissolved in oil-filled power transformers (or accumulate as free gases if produced rapidly in large quantities). The presence of these gases, called characteristic dissolved gas of oil, can directly influence the operation status in the equipment, indicating the ageing process and material deteriorating

* Corresponding author.
E-mail address: talita.mazon@cti.gov.br (T. Mazon).

https://doi.org/10.1016/j.matchemphys.2023.128576
Received 24 July 2023; Received in revised form 6 October 2023; Accepted 15 October 2023
Available online 16 October 2023

and its detection can help prevent further damage in the equipment. Thus, it is important to develop sensor devices for real-time monitoring to early detection of transformer faults, performing *in situ* measurements of these dissolved gases in transformer oil [1–4].

With the increase of scientific and industrial interest, in recent years the research for the development of online systems for diagnosis and monitoring of equipment in the electricity distribution and transmission system has grown, mainly due to structural changes in this sector that promote competition and require more rigorous indexes of quality and service. Due to rapid development of nanotechnology, various technologies applied for nanoscale materials with gas sensing property, such as the use of metal oxide (MO) semiconductor, such as SnO_2, ZnO, In_2O_3 and TiO_2 [5–9] have gained attention due to its production versatility, detection of many harmful gases with high sensitivity (including CO), simple operation and fabrication, high stability, long service life, low maintenance cost, fast response and recovery time [10–12].

The MO-based sensors operate by utilizing the change in the band gap, which is the energy range between the valence and conduction bands, due to the interaction between the gas molecules and the metal oxide surface, leading to alterations in the conductivity of the device. These alterations result from processes such as gas adsorption, ionization of gas atoms, or chemical reactions with the sensor material. By monitoring the variation in the electrical resistance sensor, it becomes possible to infer the presence and concentration of the gas being analyzed. This electrical signal can be processed and converted into a quantitative reading, providing valuable information for gas detection and monitoring across various applications [13–15]. Carrying out the monitoring of the gases dissolved into the oil is important to obtain parameters that indicate a functional abnormality in the transformer, such as useful life and safety of the transformers, the severity and type of failures [16–18].

The SnO_2-based materials is currently the one of promising studied sensing devices for dissolved gas analysis (DGA) in experimental research and commercial application for detection of gases produced on transformer oil [18–20]. The focus are on synthesis and preparation methods and also by carrying out doping with noble metals (such as platinum, palladium, gold, rhodium) to improve gas sensor performances, based on the modification of material resistance [21–26].

In Table 1 we summarize some types of sensor used for CO detection. As it can be observed, many different materials (produced by different methods) can be used for carbon monoxide monitoring. Almost all papers are related on determine the gas sensing properties using an atmospheric chamber with gas injection and a heating system for improvement of the sensibility and response/recovering time. The development of oil-immersed sensors plays a crucial role in many areas, contributing to the safety, efficiency, and reliability of industrial processes and critical systems. As technologies advance, it is expected that these sensors will become more sensitive, stable, and versatile, catering to a wide range of needs across various industries.

The significant importance of oil-immersed sensors lies in providing real-time information, and these are essential considerations. Researchs related to devices for *in situ* measurements are in its early stages (within the last 2 years), where some available articles focus on density functional theoretical studies (DFT) of promising materials or in a chamber inside the transformer system (not immersed) without making contact with the oil (in this case it is necessary to wait for molecules of the generated gas to be transferred to the headspace, according to the principle of chemical equilibrium). Material such as Pt-doped $MoTe_2$ [27], Cu-embedded $PtSe_2$ [28], Ir-decorated MoS_2 [29], Pd_4-SnO_2 [30] and Cu-decorated ZnO [31] have been study to understand the adsorption mechanism and sensing behaviors. The DFT method is used to calculate the geometric optimization, binding energy, adsorption energy, charge transfer, density of states, band structure, deformation charge density difference, total charge density, and molecular orbital [27–31]. The papers provide some guidance for the preparation of these materials to overcome challenges like sensitive material discovery, coating usage, calibration, detection technique, stability, and integration into systems.

The aim of this present study was the development of a room temperature gas sensor device based on a monolayer of SnO_2 deposited through printing technique, decorated on the surface with Pd metallic NP. To determine the sensing property, it was investigated and characterized the electrical behavior of the prepared electrode immersed into mineral oil for *in situ* detection of CO gas resulting from injection in

Table 1
– Sensing characteristics comparison between CO gas based sensors reported in the literature.

Material	Procedure	[CO] in ppm	Temperature (°C)	Analysis	Property investigated	Result	Ref.
TiO_2/CeO_2 nanosheet	Hidrothermal synthesis Flame anneling	0.5	300	Atmosphere chamber	Electrical Resistance	6 s of recovering time	[32]
Pt-In_2O_3 nanoparticles	Hidrothermal synthesis Inkjet printing	250	200	Atmosphere chamber	Electrical Resistance	35 s of response time 25 s of recovering time	[33]
$LaNbO_4$	Solid state reaction Tape casting	400	400	Atmosphere chamber	Electrical Resistance	47 s of response time 52 s of recovering time	[34]
Au-dcorated Sb-WS_2	Propanal dispersion Drop casting	50	140	Atmosphere chamber	Electrical Resistance	Sensor Response of 3.9 at 4.8 V	[35]
Pd-loaded SnO_2	Microwave assisted hidrothermal synthesis Coating on ceramic tube	10	100	Atmosphere chamber	Electrical Resistance	Sensor Response of 1.5 60 s of response time 150 s of recovering time	[36]
ZnO:Au	RF Sputtering	20	250	Atmosphere chamber	Electrical Resistance	Sensor Response of 6.4 11 s of response time	[37]
SnO_2:Ni	Screen printing	250	375	Atmosphere chamber	Electrical Resistance	Sensor Response of 40 6 s of response time 39 s of recovering time	[38]
SnO_2-Mn_3O_4 composite	Hydrothermal synthesis Screen-printing	400	350	Atmosphere chamber	Electrical Resistance	Sensor Response of 1.1	[39]
Pt-SnO_2	Sol-gel method	300	200	Atmosphere chamber	Electrical Resistance	Sensor Response of 795 8 s of response time	[40]
TiO_2 with multi-walled carbon nanotubes	Sol-gel/Solvothermal	50	300	Atmosphere chamber	Electrical Resistance	Sensor Response of 15.8 4 s of response time 16 s of recovering time	[41]
Cu nanocubes	Thermal oxidation	100	175	Atmosphere chamber	Electrical Resistance	Sensor Response of 1.13 13 s of response time 12 s of recovering time	[42]

a headspace chamber and its dissolution in the analyzed oil.

2. Experimental procedure

2.1. Materials

All chemicals were of analytical grade, commercially available, and had not been further purified or processed. In this research it were used the reagents: tin (II) chloride ($SnCl_2$ - Sigma-Aldrich), ammonium hydroxide (NH_4OH - Dinâmica), sodium tetrachloropalladate (Na_2PdCl_4 - Sigma-Aldrich), polyvinyl pyrrolidone (PVP $(C_6H_9NO)_n$ - Sigma-Aldrich), Diethylene glycol (Synth), polyvinylidene difluoride (PVDF - Sigma-Aldrich), n-methyl pyrrolidone (NMP - Sigma-Aldrich).

2.2. Synthesis of SnO_2 and Pd NPs

The SnO_2 powder was synthesized from solution 0.25 M of $SnCl_2$ and addition of 0.27 mol of NH_4OH until pH ~9. The obtained precipitate of $Sn(OH)_2$ was centrifuged (12000 rpm during 30 min), washed with distilled water, dried at 100 °C (overnight) and then calcined at 400 °C/4 h.

The Pd NPs were synthesized using 2 different solutions: (1) First, by solubilizing polyvinylpyrrolidone (PVP) in diethylene glycol under magnetic stirring, then this solution was put in to a volumetric flask coupled to a reflux system and heated to 160 °C, under stirring; (2) by the dissolution of sodium tetrachloropallate (Na_2PdCl_4) in diethylene glycol in an ultrasonic bath. The solution (2) was added into the reflux flask containing the PVP solution (1) at 160 °C and kept under stirring for 1 h. The flask was removed from the reflux system and cooled in an ice bath. Then, the solution was centrifuged (12000 rpm for 10 min) and washed with isopropyl alcohol until total suspension clearing and precipitation of Pd NPs.

2.3. SnO_2:Pd electrode

To prepare the sensor device it was used a commercial sensor board containing gold interdigital electrode (IDE) made of alumina substrate (30 × 6 mm size) with an inter-spacing gold trail of 150 μm, as shown in Fig. 1. The previously prepared SnO_2 nanoparticles were mixed with 5% of PVDF (w/w) using NMP as solvent to form a paste.

Through the screen-printer method the paste was deposited 4 times on the sensor board to form a homogeneous layer, followed by drying at 120 °C/10 min. Then, 2 aliquots of 20 μL from the previously prepared Pd-NPs suspension ([Pd] = 0.26 mg mL^{-1}) was deposited, with an interval of 5 min and drying at 120 °C, onto the SnO_2-paste. Finally, the sensor board was dried overnight in the vacuum oven at 100 °C, followed by heat treatment at 300 °C/4 h in a muffle furnace at air atmosphere.

2.4. Characterizations

The crystal structure of the samples was characterized by XRD from XRD7000 Shimadzu X-ray diffractometer (2θ = 10–80° of range with increment of Δ2θ = 0.02°, CuKα radiation, λ = 1.5460 Å). The results were compared to JCPDS card patterns. The morphology of the samples was analyzed by SEM from Tescan model Mira 3 XMU, thus making a qualitative morphological analysis of the powders. Raman Spectroscopy measurements were made in Raman Horiba Jobin Yvon Spectrometer, model T64000, within the spectral range of 100–4000 cm^{-1} (5 scans) and using a 532 nm laser.

2.5. Gas sensor set up and measurements

For this analysis LUBRAX AV 70 IN insulating mineral oil was used, produced by Petróleo Brasileiro S.A (Petrobrás), a naphthenic mineral base (aromatic hydrocarbon with molecular formula $C_{10}H_8$) and inhibited with BHT antioxidant, for use in transformers of all voltage classes, circuit breakers and switching equipment. The oil is produced through a severely hydrotreatment and shows a low power factor associated with high oxidation stability. To the product is added 0.3% (w/w) of the BHT (DBPC) antioxidant. No other additives are incorporated, which is totally free of contamination with PCBs (polychlorinated biphenyls) or other chlorinated products.

The equipment used to measure the sensor sensitivity is shown in Fig. 2. A mixture of N_2 and CO is continuously injected into one of the chambers, directly into the oil through a bubbler built by a sintered stainless steel filter with a 10 μm passage, in order to produce rapid solubilization and equilibrium of the gases in the oil. The CO concentration is controlled by controlling the N_2 flow rates (mass flow control MKS-GE50A) and a previously calibrated N_2/CO mixture.

The two chambers are connected at the height of the liquid level so that both the head space and the liquid phase of the chambers are interconnected. A recirculation pump (RP) to ensure good mixing of the liquid from the gas injection chamber to the measurement chamber where the sensor is located. Excess gas from the head space exits through a vent where it is possible to monitor the gas flow rate (100 mL/min). Continuous injection of the gas mixture ensures constant CO concentration in the headspace. The concentration of dissolved CO is calculated by the Ostwald coefficient (0.133 for CO gas).

The measurement of dissolved gas by measuring the gas in the headspace is accepted as a reliable measurement in accordance with the IEC 60567 standard. Several methods of measuring dissolved gas concentration have been developed [43–46], but the complexity of these methods does not yet allow for a direct measurement and such methods

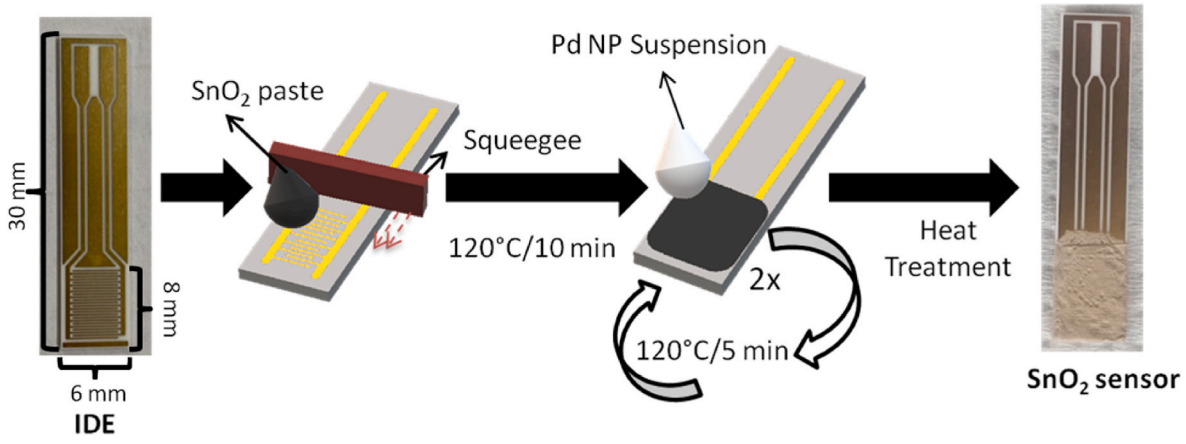

Fig. 1. – Procedure to deposit samples on commercial sensor board.

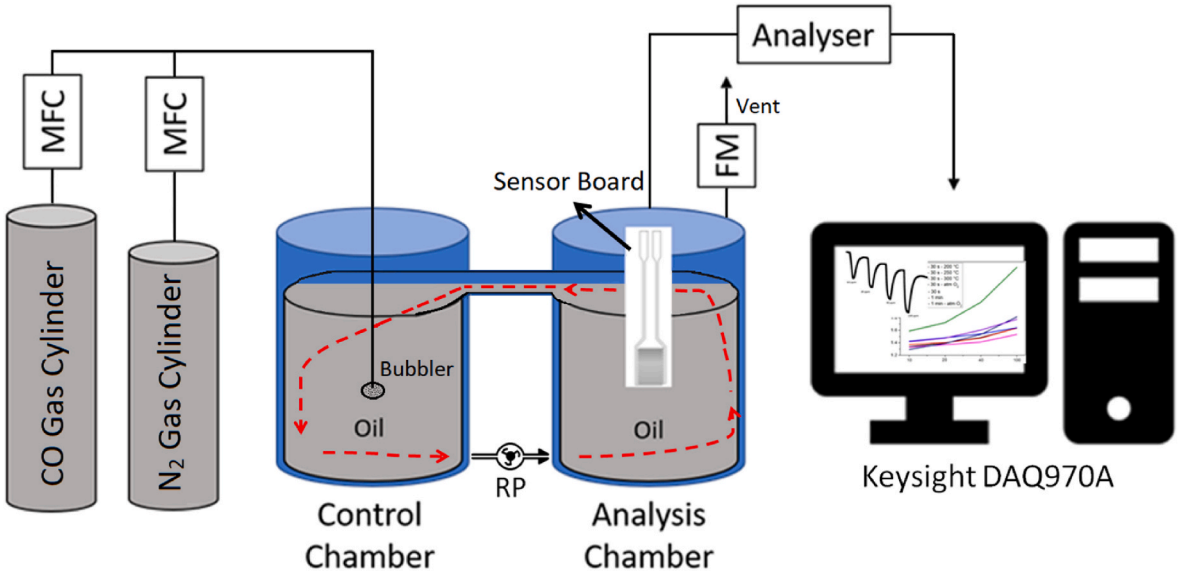

Fig. 2. – Simplified scheme of the equipment used for analysis of CO dissolved gas in transformer oil. (RP = recirculation pump).

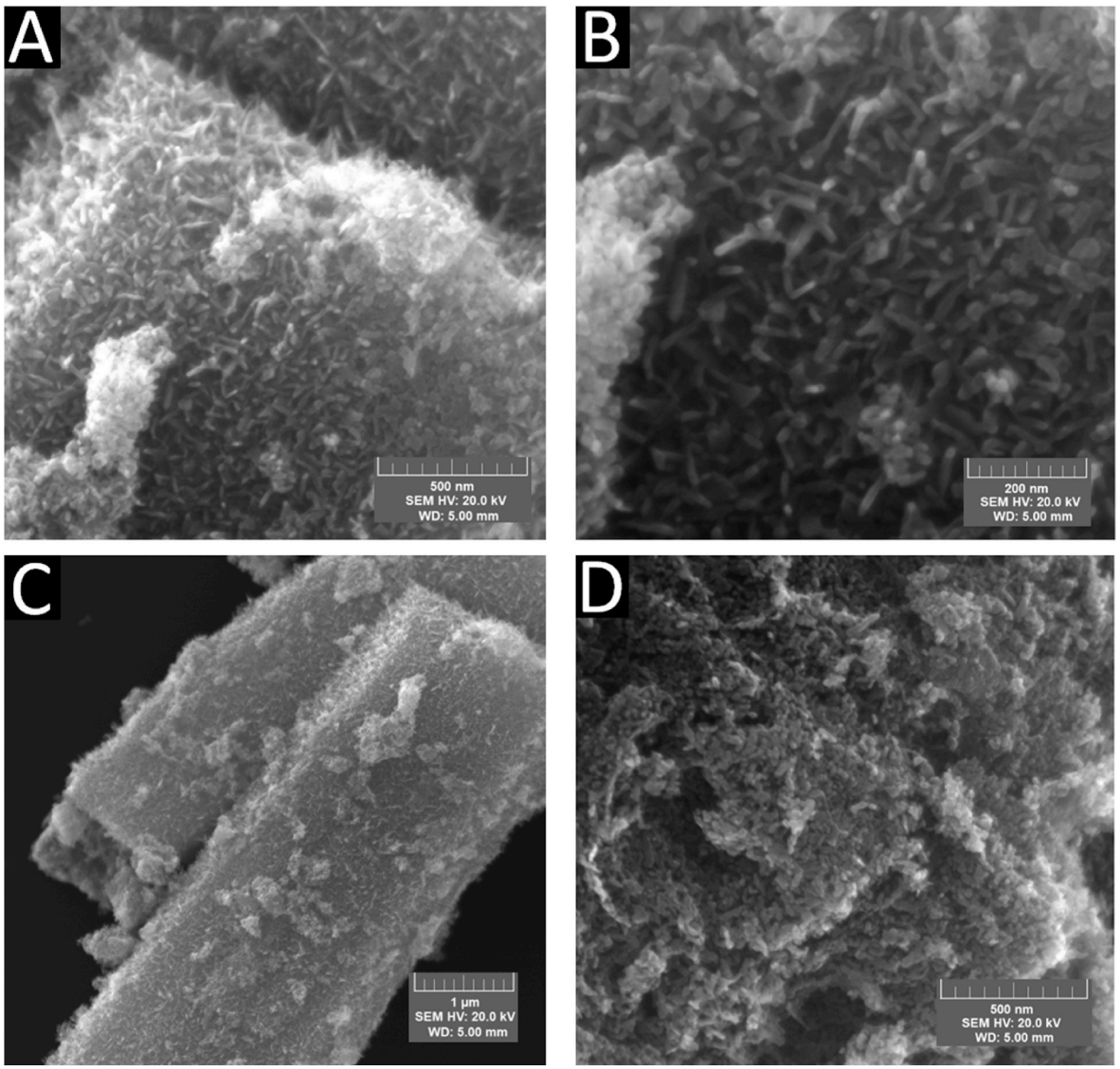

Fig. 3. – SEM images for SnO_2 as-synthesized powder. Different magnifications.

are mainly used to determine the Ostwald and Henry's law coefficients.

Gas Sensing analyzes was performed with the sensor board submerged into the oil at room temperature and varying the concentration range from 0 to 500 ppm of carbon monoxide in the headspace of the Control Chamber. Each concentration condition was injected into the control chamber for 2 h to promote its dissolution in the oil. N_2 was used as purge gas during 4 h to clean the system. The sensitivity was measured by the variation on the sensor resistance analyzed by a Keysight DAQ970A.

3. Results and discussion

3.1. Morphological and structural investigation

The morphology of particles has an important function in the gas sensing property to improve the chemical interaction between the adsorbed gas and the semiconductor. Trough SEM in Fig. 3, it was possible to observe the formation of agglomerates of irregular size (~3–10 μm), as showed in the as-synthesized SnO_2 powder, which are favored due to the attractive forces between the individual particles. When particles are synthesized with nanometer sizes, they present a high surface energy and, therefore, a great tendency to aggregate with each other to minimize this energy from the system. For the tin dioxide nanoparticles it was observed that particles had size in nanometer scale and shape as rods (diameter range of 10–15 nm, analyzed by ImageJ software).

Fig. 4 shows a top view from the base sensor after palladium deposition as indicated in procedure 2.3 item. It was verified an irregular surface and also the microsized SnO_2 agglomerates was again observed. From qualitative analysis of EDS (Fig. 4-B) it was possible to indentify the Pd NPs and observe its homogeneous distribution on SnO_2 surface particles through deposition drop casting. The Pd-NP has spherical shape with calculated diameter in a range of 15–35 nm, analyzed by ImageJ software.

XRD technique was used to investigate the crystalline phase and purity of the as-synthesized samples. Fig. 5A shows the diffract pattern

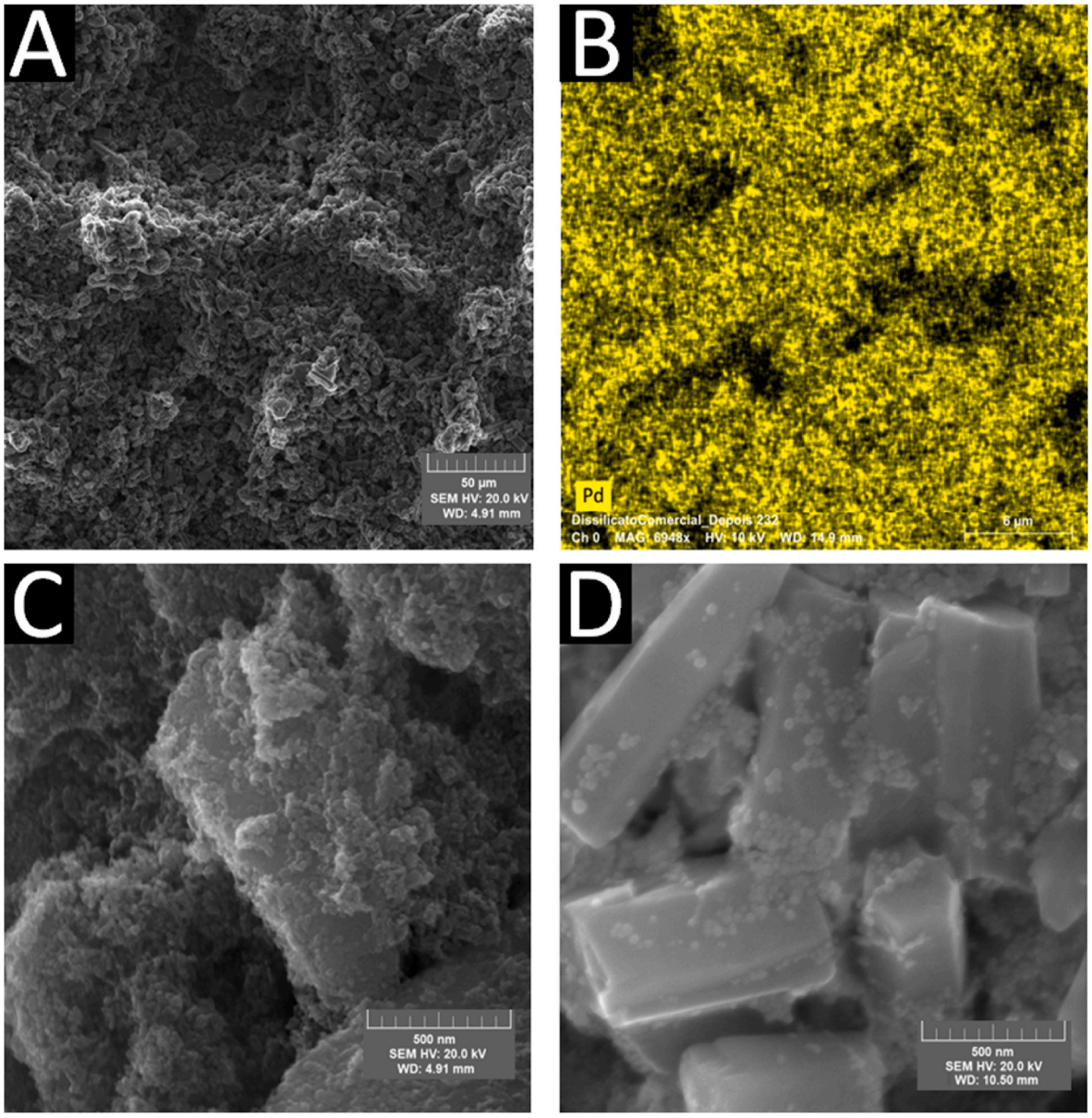

Fig. 4. – Top view of SEM images and EDS mapping color for SnO_2:Pd sensor board. Different magnifications. (For interpretation of the references to color in this figure legend, the reader is referred to the Web version of this article.)

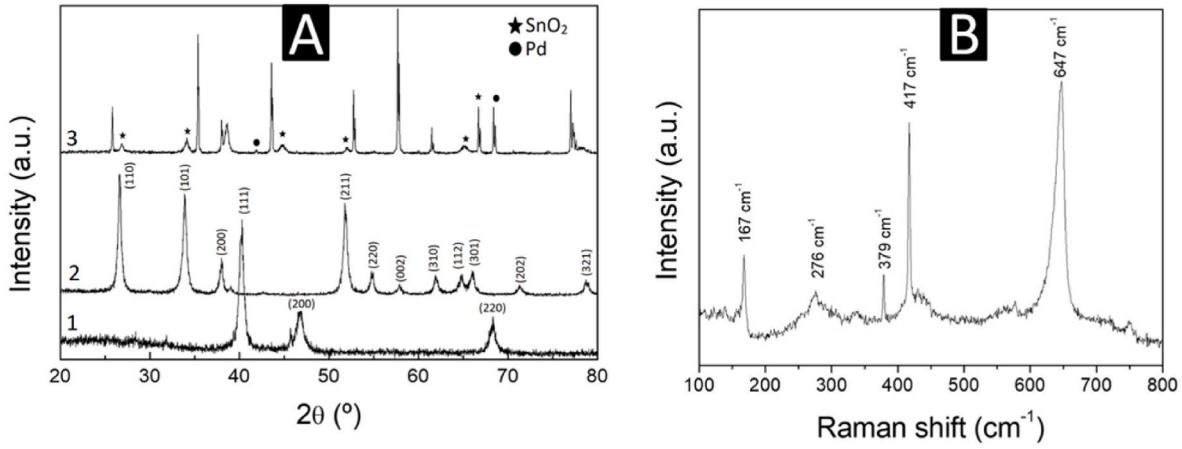

Fig. 5. – (A) XRD analysis of (1) Pd, (2) SnO_2 nanoparticles and (3) SnO_2:Pd-sensor board; and (B) Raman spectra of SnO_2:Pd-sensor board.

of SnO_2 and Pd NPs. As observed, the samples have diffraction peaks can be well indexed to the rutile tetragonal structure of SnO_2-cassiterite phase according to JCPDS-ICDD card nº 41–1445 [47–49] and the cubic structure of Pd NPs according to card nº 46–1043 [50]. The narrow peaks indicate good crystallinity and high purity of the material. In addition, it didn't detect peaks from other phases segregated or other impurities. After deposition of as-synthesized powders on sensor board, as described in item 2.4, the device was characterized by XRD (shown in Figs. 5A–3). Here it is also possible to identify peaks related to both SnO_2-tetragonal and Pd-cubic structures, the unidentified peaks (of high intensity) match the alumina substrate profile [51].

Therefore we have studied the vibration properties of prepared samples by Raman spectroscopy, shown in Fig. 5B. The SnO_2:Pd composite exhibited two characteristic vibration modes of A_{1g} at around 647 cm^{-1} (related to contractions and expansions of Sn–O bonds) and E_g, at around and 417 cm^{-1} (characteristic of the translational movement of the oxygen atom), which confirmed the rutile structure of SnO_2. The observance of the related peak at 379 cm^{-1} indicates a level of disorder in the crystal lattice and oxygen vacancies [52–55]. We also observed low intensity peaks related to inactive vibration modes of E_u and A_{2g}, located at around 330 and 550 cm^{-1}, respectively, which have been ascribed to the existence of oxygen vacancies in rutile SnO_2. These vacancies could be classified as types of subbridging and bridging, oxygen vacancies, responsible for E_u and A_{1g} modes, respectively. The peak intensities of these modes are proportional to the density of oxygen vacancies [56–58].

3.2. Gas sensing measurements and mechanism

The gas sensing mechanism for SnO_2 can be explained by a general model for n-type metal oxide. The sensor response is related to the change in semiconductor resistivity due to the adsorption/desorption of the gas molecules in these materials, leading to a modification of the electron density in the grain boundary region formed in this junction. This effect can be enhanced by electrical activities due to the electron-hole pairs (e^-/h^+) on the oxide material surface [59–61].

In the case of the SnO_2 sensor immersed in naphthenic-based mineral oil, the aromatic molecules present in the oil can be adsorbed on the surface of the SnO_2 and this interaction can transfer some electrons to SnO_2 grain and increase the electronic mobility (conductivity) of sensor by decrease of the potential barrier, as schematized in Fig. 6-A. From the introduction of CO gas into the headspace of the analysis chamber and its dissolution into the oil, according to the Ostwald coefficient, a chemical reaction takes place between the dissolved gas molecules and the surface of the SnO_2, trapping the electrons from conduct band. This reaction causes a change in the amount of free electrons present on the surface of SnO_2, and, consequently, a change in its electrical conductivity, increasing both the depletion layer (a region where no mobile charge carriers are present) and the potential barrier at grain boundary region which leads to a decrease of the electronic conduction from the sensor, as schematized in Fig. 6-B. [12,62].

Generally the signal responses of metal oxide based sensors are not linear, that is, they have some small signal deviations in their response that are acceptable within a limited range. The sensor response (R) is mostly related to the variation of its resistance in the presence of molecules of the analysis gas (reducing or oxidizing atmosphere) and its defined concentration. The sensor signal (S) is used to create a relationship between the sensor responses (R), as shown in Equation (1). [10,63].

$$S_{red} = \frac{R_{gas}}{R_0} \leq 1 \; and \; S_{ox} = \frac{R_{gas}}{R_0} \geq 1 \tag{1}$$

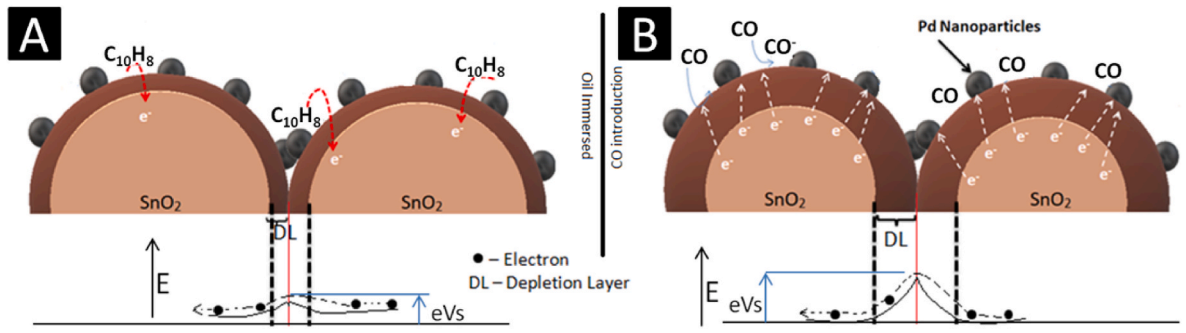

Fig. 6. – Representation of SnO_2 grain interface and the potential barrier (A) immersed in a mineral oil and (B) after CO gas injection in the system followed by dissolution into the oil.

where R_0 and R_{gas} represent the resistances sensor in absence and presence in the test gas, respectively; the S_{red} and S_{ox} is the signal sensor at reducing (i.e. when the resistance decreases) and at oxidizing atmosphere (i.e. when the resistance increases), respectively.

Bechthold et al. [64] conducted a study about adsorption of CO molecules on Pd-SnO_2 surface by DFT calculations and Density of Sates curves to analyze the electronic structure. The CO adsorption may occur in three ways, in order of preference: top bonded to the Pd atom, laterally bonded to the Pd atom and to a Sn top geometry. In all cases there are transfers charges from the surface to the CO molecule. In both top and laterally interaction of Pd-C the bridging oxygen atom from SnO_2 increase (Pd-O1 distance), thus shortening the Pd-C distance, corresponding to a stronger adsorption of CO on palladium nanoparticles, improving the sensor response.

In our experiments, the SnO_2:Pd sensor board was immersed in the mineral oil, base of naphthalene molecules ($C_{10}H_8$), composed of two aromatic structures, having a charge density in the electronic cloud with 10 delocalized π-electrons. The molecules are adsorbed in the surface of tin oxide and thus promote the electron interaction that lead to a decrease of the depletion layer and consequently its resistance, continuously, as indicated in Fig. 7-A which represents the blank analysis, for 40 h, from resistance measurements carried out only by immersion time without any injection of CO gas. It is possible to observe a continuous decrease in baseline of resistance due to naphthenic electrons interacting with the sensing surface. So, when the CO dissolved gas adsorb on grains, the molecules will trap electrons from the surface, promoting an increasing depletion layer formed at the grain boundary, and then its detection is observed by rising of the resistance, as showed in Fig. 7-B.

As observed in Table 2, the first two analysis conditions, in fact, represent too low concentration of CO dissolved, according to the Ostwald solubility coefficient (0.133 for carbon monoxide gas), and our system does not show change by increasing the resistance, only the continuous decrease from the baseline by the interactions of $C_{10}H_8$ molecules on SnO_2:Pd-sensor board. When 200 ppm of CO gas was injected in the Control Chamber headspace (i.e. 26.6 ppm dissolved into oil), the signal resistance has its perceptible change.

As we carry out the *in situ* analysis, long injection times (2 h) were required to promote the dissolution and homogenization of the gas into the oil, and even longer purge gas times (4 h) for complete cleaning/remotion of the adsorbed molecules from analyzed gas. In that regard, the 500 ppm parameter was only started after almost 35 h of the experiment, and we did not have a response in the resistance. As it is possible to observe, after 30 h, there is only a linear decrease of signal, indicating that the material may have worn out due to the long time interaction with the analysis environment, caused by the adsorption of naphthalene molecules on the surface of the SnO_2 grains, thus requiring stronger cleaning steps or even changing the electrode.

Table 2
– Corrections of CO concentration into oil by Ostwald solubility coefficient.

[CO] injected in Headspace (ppm)	[CO] in Oil by Ostwald coefficient (ppm)
50	6.65
100	13.3
200	26.6
300	39.9
400	53.2
500	66.5

In Fig. 8-A is plotted the normalized curves of signal response (R_{gas}/R_0) for others samples prepared in triplicate by the same procedure in this study, named as Sensor 1, Sensor 2, and Sensor 3. In this graph we can see a little variance of signal after 100 ppm (13.3 ppm of CO gas dissolved into oil), which can be attributed to deviations of baseline stabilization, but in 200 ppm (26.6 ppm of CO gas dissolved into oil) the variance in resistance indicate the detection of CO gas in the oil, more accentuated when the analyzed concentration is 53.2 ppm. Fig. 8-B shows a fit linear for curves of electric response of SnO_2 when CO was dissolved into the analyzed mineral oil. The values of resistance are presented in Table 3. In this graph, an error bar was added to each curve according to its standard deviation (70.017, 158.274 and 77.337 for Sensor 1, Sensor 2 and Sensor 3, respectively). Error bars allow us to assess uncertainty in the results and determine whether differences between curves are statistically significant. The high R^2 values (>0.9) for Sensor 2 and 3 indicate a good fit for linear decrease according the CO concentration increases. However, Sensor 1 presents a lower linearity, which may be due to factors such as variations in the sensitivity of this specific sensor. The implications of these results for the use of SnO_2 sensors for the detection of CO in mineral oil are that the sensors must be calibrated regularly and that it is important to consider the uncertainty in the results when interpreting the results.

Currently, in industrial settings the gas analysis is performed at 6-month intervals using gas chromatography (GC). This technique is a widely used analytical technique for the identification and quantification of dissolved gases in oil. However, GC can fail to provide accurate results if the analysis time is too long. This is because dissolved gases in oil are volatile and can be lost to the atmosphere. The analysis time can increase the rate of gas loss, resulting in an underestimation of the gas concentration in the sample. The primary focus of this paper is not on determining the precise gas concentration, but detection capability when immersed in oil, as even the slightest concentration indicates operational failure and warrants prompt equipment repair. By employing sensors of this type, real-time analysis becomes feasible, eliminating the risk of significant failures that may occur during the six-month gap between chromatography analyses.

In our paper, we primarily focused on the detection of CO using the studied sensor. However, it is worth noting that others gases are

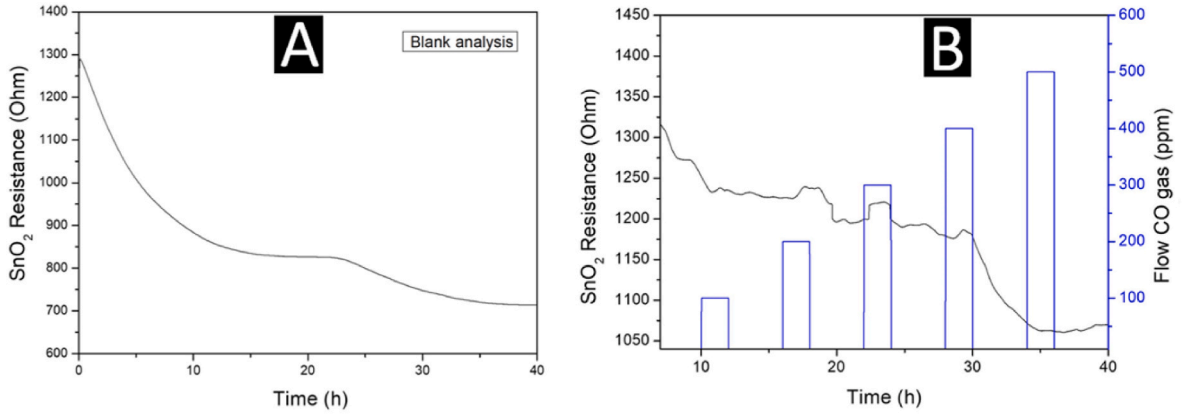

Fig. 7. – Sensor response of SnO_2:Pd sensor board (A) without and (B) at different CO gas concentrations.

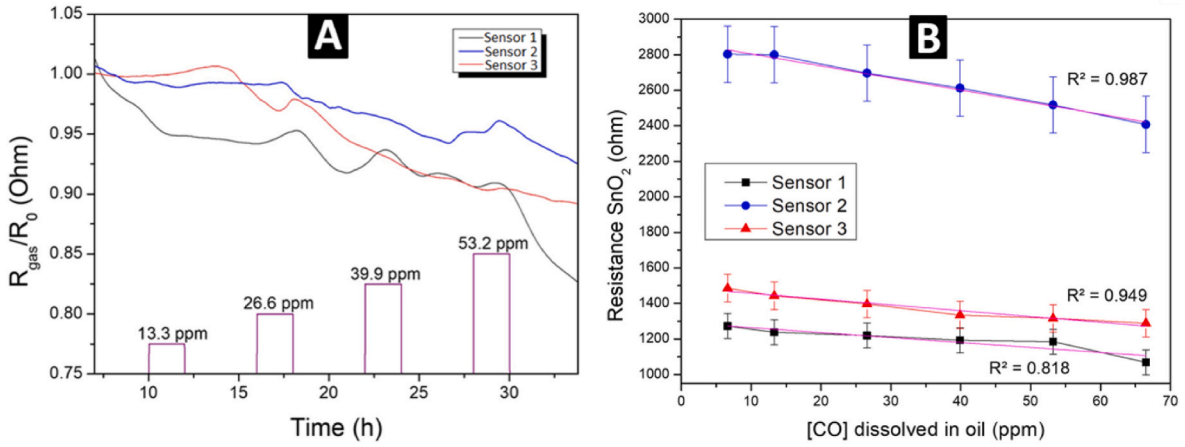

Fig. 8. – (A) Normalized curves of sensor signal (R_{gas}/R_0) and (B) calibration curves of resistance response according to real gas concentration determined by Ostwald coefficient.

Table 3
– Electrical response (R) for SnO_2:Pd based samples submitted to a different low concentrations of carbon oxide.

[CO] ppm	Electrical Resistance (Ohm)			
Sensor	13.3	26.6	39.9	53.2
Sensor 1	1237.35	1219.26	1192.64	1184.53
Sensor 2	2800.22	2696.26	2611.64	2517.51
Sensor 3	1442.84	1396.86	1334.75	1315.56

commonly found in real transformer oil and can potentially interact with the sensor as well. These gases have different solubility coefficient and may have different levels of reactivity and adsorption characteristics compared to CO. Further investigation and experimentation are been conduced, involve assessing the sensor's response to individual gases and their combinations (mixing the gases), studying their adsorption behavior, and analyzing the potential cross-reactivity or selectivity of the sensor towards different gases. We will also assess the sensor's shelf life to determine its durability and efficiency in detecting the gas over multiple reuse cycles.

4. Conclusions

This research showcases the potential of the SnO_2-sensor board with palladium metallic nanoparticles for effectively monitoring and detecting CO dissolved in mineral oil, even at trace levels. The results open doors to further advancements in the field of gas detection and provide valuable insights for developing proactive maintenance strategies in critical systems.

In our study, we developed a sensor based on SnO_2 with Pd metallic NPs deposited on its surface. The aim was to investigate the detection of CO gas dissolved in naphthenic base mineral oil by monitoring changes in electrical conductivity. When the SnO_2:Pd sensor board was immersed in mineral oil, a clear correlation was observed between the presence of CO and the corresponding change in electrical conductivity of the sensor device. Notably, even at very low concentrations (as low as 13.3 ppm, as per the Ostwald solubility coefficient), the SnO_2 sensor demonstrated sensitivity to the presence of CO dissolved in the mineral oil.

CRediT authorship contribution statement

Agnes Nascimento Simões: Formal analysis, Investigation. **Glauco Meireles Mascarenhas Morandi Lustosa:** Formal analysis, Writing – original draft, Writing – review & editing, Visualization. **Eugênio de Souza Morita:** Formal analysis, Investigation. **André Nunes de Souza:** Conceptualization, Methodology. **Floriano Torres:** Project administration. **Waldir Antonio Bizzo:** Conceptualization, Methodology, Writing – review & editing. **Talita Mazon:** Conceptualization, Methodology, Writing – review & editing, Supervision, Project administration, Funding acquisition.

Declaration of competing interest

The authors declare that they have no known competing financial interests or personal relationships that could have appeared to influence the work reported in this paper.

Data availability

Data will be made available on request.

Acknowledgement

The authors thanks to the financial support of this project by CPFL group through the Research and Development Project PD-00063-3067/2019 with resources from ANEEL's R&D program, and by the CNPq-Conselho Nacional de Desenvolvimento Científico e Tecnológico and FAPESP-Fundação de Amparo à Pesquisa do Estado de São Paulo (CEPID-CDMF 2013/07296-2). The authors would also like to thank CTI-Nano, the strategic laboratory from SisNano and MCTI, and the laboratory of the microscopy—CNPEM, for their support of this research.

References

[1] H. Cui, D. Chen, Y. Zhang, X. Zhang, Dissolved gas analysis in transformer oil using Pd catalyst decorated MoSe2 monolayer: a first-principles theory, Sustain. Mater. Technol. 20 (2019), e00094, https://doi.org/10.1016/j.susmat.2019.e00094.
[2] H. Zhang, W.G. Chen, Y.Q. Li, Z.H. Song, Gas sensing performances of ZnO hierarchical structures for detecting dissolved gases in transformer oil: a mini review, Front. Chem. 6 (2018) 1–7, https://doi.org/10.3389/fchem.2018.00508.
[3] T. Jiang, W. Zhang, T. Zhang, H. Yuan, M. Bi, X. Zhou, Adsorption and gas-sensing performances of C2H2, C2H4, CO, H2 in transformer oil on Pt-doped MoTe2 monolayer: a DFT study, Phys. E Low-Dimensional Syst. Nanostructures. 146 (2022), 115568, https://doi.org/10.1016/j.physe.2022.115568.
[4] J. Ding, X. Li, J. Cao, L. Sheng, L. Yin, X. Xu, New sensor for gases dissolved in transformer oil based on solid oxide fuel cell, Sensor. Actuator. B Chem. 202 (2014) 232–239, https://doi.org/10.1016/j.snb.2014.05.061.
[5] J. Fan, F. Wang, Q. Sun, H. Ye, Q. Jiang, Application of polycrystalline SnO2 sensor chromatographic system to detect dissolved gases in transformer oil, Sensor. Actuator. B Chem. 267 (2018) 636–646, https://doi.org/10.1016/j.snb.2018.04.014.

[6] Q. Zhou, W. Chen, L. Xu, S. Peng, Hydrothermal synthesis of various hierarchical ZnO nanostructures and their methane sensing properties, Sensors 13 (2013) 6171–6182, https://doi.org/10.3390/s130506171.

[7] G. Xiao, W. Chen, S. Peng, C. Yu, Z. Jiang, Competitive adsorption of gases dissolved in transformer oil on Co-doped ZnO (0 0 0 1) surface, Comput. Mater. Sci. 142 (2018) 72–81, https://doi.org/10.1016/j.commatsci.2017.10.004.

[8] Y. Gui, W. Li, X. He, Z. Ding, C. Tang, L. Xu, Adsorption properties of pristine and Co-doped TiO2(1 0 1) toward dissolved gas analysis in transformer oil, Appl. Surf. Sci. 507 (2020), 145163, https://doi.org/10.1016/j.apsusc.2019.145163.

[9] Y. Cao, J. Zhao, X. Zou, P.-P. Jin, H. Chen, R. Gao, L.-J. Zhou, Y.-C. Zou, G.-D. Li, Synthesis of porous In2O3 microspheres as a sensitive material for early warning of hydrocarbon explosions, RSC Adv. 5 (2015) 5424–5431, https://doi.org/10.1039/C4RA13763A.

[10] S. Zhu, Y. Liu, G. Wu, L. Fei, S. Zhang, Y. Hu, Z. Yan, Y. Wang, H. Gu, W. Chen, Mechanism study on extraordinary room-temperature CO sensing capabilities of Pd-SnO2 composite nanoceramics, Sensor. Actuator. B Chem. 285 (2019) 49–55, https://doi.org/10.1016/j.snb.2019.01.027.

[11] T. Hyodo, M. Takamori, T. Goto, T. Ueda, Y. Shimizu, Potentiometric CO sensors using anion-conducting polymer electrolyte: effects of the kinds of noble metal-loaded metal oxides as sensing-electrode materials on CO-sensing properties, Sensor. Actuator. B Chem. 287 (2019) 42–52, https://doi.org/10.1016/j.snb.2019.02.036.

[12] M.H. Kim, B. Jang, W. Kim, W. Lee, Enhanced hydrogen sensing properties of Pd-coated SnO2 nanorod arrays in nitrogen and transformer oil, Sensor. Actuator. B Chem. 283 (2019) 890–896, https://doi.org/10.1016/j.snb.2018.12.063.

[13] Y. Masuda, Recent advances in SnO2 nanostructure based gas sensors, Sensor. Actuator. B Chem. 364 (2022), 131876, https://doi.org/10.1016/j.snb.2022.131876.

[14] B. Li, Q. Zhou, S. Peng, Y. Liao, Recent advances of SnO2-based sensors for detecting volatile organic compounds, Front. Chem. 8 (2020) 1–6, https://doi.org/10.3389/fchem.2020.00321.

[15] A. Mirzaei, H.R. Ansari, M. Shahbaz, J.Y. Kim, H.W. Kim, S.S. Kim, Metal oxide semiconductor nanostructure gas sensors with different morphologies, Chemosensors 10 (2022), https://doi.org/10.3390/chemosensors10070289.

[16] A.A. Alharbi, A. Sackmann, U. Weimar, N. Bârsan, A highly selective sensor to acetylene and ethylene based on LaFeO3, Sensor. Actuator. B Chem. 303 (2020), 127204, https://doi.org/10.1016/j.snb.2019.127204.

[17] M.S. Park, J.H. Lee, Y. Park, R. Yoo, S. Park, H. Jung, W. Kim, H.S. Lee, W. Lee, Doping effects of ZnO quantum dots on the sensitive and selective detection of acetylene for dissolved-gas analysis applications of transformer oil, Sensor. Actuator. B Chem. 299 (2019), 126992, https://doi.org/10.1016/j.snb.2019.126992.

[18] J. Fan, F. Wang, Q. Sun, F. Bin, H. Ye, Y. Liu, An online monitoring system for oil immersed power transformer based on SnO2 GC detector with a new quantification approach, IEEE Sensor. J. 17 (2017) 6662–6671, https://doi.org/10.1109/JSEN.2017.2734072.

[19] H. Zhang, Z. Li, L. Liu, X. Xu, Z. Wang, W. Wang, W. Zheng, B. Dong, C. Wang, Enhancement of hydrogen monitoring properties based on Pd–SnO2 composite nanofibers, Sensor. Actuator. B Chem. 147 (2010) 111–115, https://doi.org/10.1016/j.snb.2010.01.056.

[20] Q. Zhou, W. Chen, L. Xu, R. Kumar, Y. Gui, Z. Zhao, C. Tang, S. Zhu, Highly sensitive carbon monoxide (CO) gas sensors based on Ni and Zn doped SnO2 nanomaterials, Ceram. Int. 44 (2018) 4392–4399, https://doi.org/10.1016/j.ceramint.2017.12.038.

[21] Q. Zhou, A. Umar, E.M. Sodki, A. Amine, L. Xu, Y. Gui, A.A. Ibrahim, R. Kumar, S. Baskoutas, Fabrication and characterization of highly sensitive and selective sensors based on porous NiO nanodisks, Sensor. Actuator. B Chem. 259 (2018) 604–615, https://doi.org/10.1016/j.snb.2017.12.050.

[22] Q. Zhou, L. Xu, A. Umar, W. Chen, R. Kumar, Pt nanoparticles decorated SnO2 nanoneedles for efficient CO gas sensing applications, Sensor. Actuator. B Chem. 256 (2018) 656–664, https://doi.org/10.1016/j.snb.2017.09.206.

[23] K. Nguyen, C.M. Hung, T.M. Ngoc, D.T. Thanh Le, D.H. Nguyen, D. Nguyen Van, H. Nguyen Van, Low-temperature prototype hydrogen sensors using Pd-decorated SnO2 nanowires for exhaled breath applications, Sensor. Actuator. B Chem. 253 (2017) 156–163, https://doi.org/10.1016/j.snb.2017.06.141.

[24] Y. Wang, Z. Zhao, Y. Sun, P. Li, J. Ji, Y. Chen, W. Zhang, J. Hu, Fabrication and gas sensing properties of Au-loaded SnO2 composite nanoparticles for highly sensitive hydrogen detection, Sensor. Actuator. B Chem. 240 (2017) 664–673, https://doi.org/10.1016/j.snb.2016.09.024.

[25] K. Inyawilert, A. Wisitsoraat, A. Tuantranont, S. Phanichphant, C. Liewhiran, Ultra-sensitive and highly selective H2 sensors based on FSP-made Rh-substituted SnO2 sensing films, Sensor. Actuator. B Chem. 240 (2017) 1141–1152, https://doi.org/10.1016/j.snb.2016.09.094.

[26] W. Lu, D. Ding, Q. Xue, Y. Du, Y. Xiong, J. Zhang, X. Pan, W. Xing, Great enhancement of CH4 sensitivity of SnO2 based nanofibers by heterogeneous sensitization and catalytic effect, Sensor. Actuator. B Chem. 254 (2018) 393–401, https://doi.org/10.1016/j.snb.2017.07.128.

[27] T. Jiang, W. Zhang, T. Zhang, H. Yuan, M. Bi, X. Zhou, Adsorption and gas-sensing performances of C2H2, C2H4, CO, H2 in transformer oil on Pt-doped MoTe2 monolayer: a DFT study, Phys. E Low-Dimensional Syst. Nanostructures. 146 (2023), 115568, https://doi.org/10.1016/j.physe.2022.115568.

[28] H. Wang, H. Wu, H. Cui, First-principles screening in Cu-embedded PtSe2 monolayer as a potential gas sensor upon CO and HCHO in dry-type transformers, Comput. Theor. Chem. 1209 (2022), https://doi.org/10.1016/j.comptc.2021.113586.

[29] H. Liu, Z. Tan, Y. Niu, S. Wang, Y. Wang, Ir-decorated MoS2 monolayer as a promising candidate to detect dissolved gas in transformer oil: a DFT study, Chem. Phys. Lett. 818 (2023) 2–8, https://doi.org/10.1016/j.cplett.2023.140410.

[30] H. Liu, F. Wang, K. Hu, T. Li, Y. Yan, Pd4 cluster decorated SnO2 nanowire for detecting characteristic gases in oil-immersed transformers: a theoretical and experimental study, Appl. Surf. Sci. 590 (2022), https://doi.org/10.1016/j.apsusc.2022.153122.

[31] Z. Pan, J. Wang, Q. Si, T. Shi, S. Ma, Cu-decorated ZnO monolayer as a promising gas sensor in dry-type transformers: a first-principles study, Comput. Theor. Chem. 1204 (2021), https://doi.org/10.1016/j.comptc.2021.113429.

[32] B. Chen, P. Li, B. Wang, Y. Wang, Flame-annealed porous TiO2/CeO2 nanosheets for enhenced CO gas sensors, Appl. Surf. Sci. 593 (2022), https://doi.org/10.1016/j.apsusc.2022.153418.

[33] S. Hong, Y. Hong, Y. Jeong, G. Jung, W. Shin, J. Park, J.K. Lee, D. Jang, J.H. Bae, J. H. Lee, Improved CO gas detection of Si MOSFET gas sensor with catalytic Pt decoration and pre-bias effect, Sensor. Actuator. B Chem. 300 (2019), https://doi.org/10.1016/j.snb.2019.127040.

[34] H. Liu, H. Yu, J. Wang, F. Xia, C. Wang, J. Xiao, LaNbO4 as an electrode material for mixed-potential CO gas sensors, Sensor. Actuator. B Chem. 352 (2022), https://doi.org/10.1016/j.snb.2021.130981.

[35] J. Kim, I. Sakaguchi, S. Hishita, T. Ohsawa, T.T. Suzuki, N. Saito, Sensors and actuators : B, Chemical Self-heated CO gas sensor based on Au-decorated Sb-implanted WS 2 nanosheets 382 (2023).

[36] Q. Wang, C. Wang, H. Sun, P. Sun, Y. Wang, J. Lin, G. Lu, Microwave assisted synthesis of hierarchical Pd/SnO2 nanostructures for CO gas sensor, Sensor. Actuator. B Chem. 222 (2016) 257–263, https://doi.org/10.1016/j.snb.2015.07.115.

[37] N. Le Hung, H. Kim, S.-K. Hong, D. Kim, Enhancement of CO gas sensing properties in ZnO thin films deposited on self-assembled Au nanodots, Sensor. Actuator. B Chem. 151 (2010) 127–132, https://doi.org/10.1016/j.snb.2010.09.036.

[38] K.-I. Choi, M. Hübner, A. Haensch, H.-J. Kim, U. Weimar, N. Barsan, J.-H. Lee, Ambivalent effect of Ni loading on gas sensing performance in SnO2 based gas sensor, Sensor. Actuator. B Chem. 183 (2013) 401–410, https://doi.org/10.1016/j.snb.2013.04.007.

[39] X.T. Yin, S.S. Wu, D. Dastan, S. Nie, Y. Liu, Z.G. Li, Y.W. Zhou, J. Li, A. Faik, K. Shan, Z. Shi, M.A. Tarighat, X.G. Ma, Sensing selectivity of SnO2-Mn3O4 nanocomposite sensors for the detection of H2 and CO gases, Surface. Interfac. 25 (2021), 101190, https://doi.org/10.1016/J.SURFIN.2021.101190.

[40] H. Mousavi, Y. Mortazavi, A.A. Khodadadi, M.H. Saberi, S. Alirezaei, Enormous enhancement of Pt/SnO2 sensors response and selectivity by their reduction, to CO in automotive exhaust gas pollutants including CO, NOx and C3H8, Appl. Surf. Sci. 546 (2021), https://doi.org/10.1016/j.apsusc.2021.149120.

[41] J.-S. Lee, T.-J. Ha, M.-H. Hong, C.-S. Park, H.-H. Park, The effect of multiwalled carbon nanotube doping on the CO gas sensitivity of TiO2 xerogel composite film, Appl. Surf. Sci. 269 (2013) 125–128, https://doi.org/10.1016/j.apsusc.2012.10.020.

[42] L. Hou, C. Zhang, L. Li, C. Du, X. Li, X.-F. Kang, W. Chen, CO gas sensors based on p-type CuO nanotubes and CuO nanocubes: morphology and surface structure effects on the sensing performance, Talanta 188 (2018) 41–49, https://doi.org/10.1016/j.talanta.2018.05.059.

[43] M.T. Imani, M. Farahani, M. Kuhnke, K. Homeier, P. Werle, Measuring methods for solubility of gases in insulation liquids, 2017 IEEE 19th Int. Conf. Dielectr. Liq. ICDL 2017 (2017) 1–4, https://doi.org/10.1109/ICDL.2017.8124654, 2017-January.

[44] J. Jalbert, R. Gilbert, P. Tétreault, M.A. El Khakani, Matrix effects affecting the indirect calibration of the static headspace-gas chromatographic method used for dissolved gas analysis in dielectric liquids, Anal. Chem. 75 (2003) 5230–5239, https://doi.org/10.1021/ac0343634.

[45] A. Muller, M. Jovalekic, S. Tenbohlen, Solubility study of different gases in mineral and ester-based transformer oils, Proc. 2012 IEEE Int. Conf. Cond. Monit. Diagnosis, C. 2012 (2012) 937–940, https://doi.org/10.1109/CMD.2012.6416307.

[46] K. Homeier, P. Werle, M. Hahn, D. Wilke, Modified dissolved gas analysis with additional detection of higher hydrocarbons for transformer faults diagnosis, Proc. - IEEE Int. Conf. Dielectr. Liq. (2022) 1–4, https://doi.org/10.1109/ICDL49583.2022.9830962, 2022-May.

[47] G.M.M.M. Lustosa, J.P. de C. da Costa, L.A. Perazolli, B.D. Stojanovic, M. A. Zaghete, Electrophoretic deposition of (Zn, Nb)SnO2-films varistor superficially modified with Cr3+, J. Eur. Ceram. Soc. 35 (2015) 2083–2089, https://doi.org/10.1016/j.jeurceramsoc.2015.01.022.

[48] A. Debataraja, D.W. Zulhendri, B. Yuliarto, Hiskia Nugraha, B. Sunendar, Investigation of nanostructured SnO2 synthesized with polyol technique for CO gas sensor applications, Procedia Eng. 170 (2017) 60–64, https://doi.org/10.1016/j.proeng.2017.03.011.

[49] T. Bilal Ahmad, A.B. Asif, wani Atif Khurshid, A.K. Masood, S. Gulzar Ahmad, Preparation and characterization of SnO2 nanoparticles for antibacterial properties, Nanomater. Chem. Technol. 2 (2020) 1–5, https://doi.org/10.33805/2690-2575.109.

[50] Z.H. Li, X.L. Zhao, X.C. Jiang, Y.H. Wu, C. Chen, Z.G. Zhu, J.L. Marty, Q.S. Chen, An enhanced nonenzymatic electrochemical glucose sensor based on copper-palladium nanoparticles modified glassy carbon electrodes, Electroanalysis 30 (2018) 1803–1811, https://doi.org/10.1002/elan.201800017.

[51] G. Gasparotto, R.A. Da Silva, M.A. Zaghete, E. Longo, L.A. Perazolli, T. Mazon, Novel route for fabrication of ZnO nanorods-Au nanoparticles hybrids directly supported on substrate and their application as gas sensors, Mater. Res. 21 (2018), https://doi.org/10.1590/1980-5373-MR-2017-0796.

[52] X. Guan, Y. Wang, P. Luo, Y. Yu, D. Chen, X. Li, Incorporating N atoms into SnO 2 nanostructure as an approach to enhance gas sensing property for acetone, Nanomaterials 9 (2019) 1–18, https://doi.org/10.3390/nano9030445.
[53] A. Birkel, F. Reuter, D. Koll, S. Frank, R. Branscheid, M. Panthöfer, E. Rentschler, W. Tremel, The interplay of crystallization kinetics and morphology during the formation of SnO2 nanorods: snapshots of the crystallization from fast microwave reactions, CrystEngComm 13 (2011) 2487–2493, https://doi.org/10.1039/C0CE00573H.
[54] G. Cheng, J. Wang, X. Liu, K. Huang, Self-assembly synthesis of single-crystalline tin oxide nanostructures by a poly(acrylic acid)-assisted solvothermal process, J. Phys. Chem. B 110 (2006) 16208–16211, https://doi.org/10.1021/jp061935q.
[55] Y. Liu, Y. Jiao, Z. Zhang, F. Qu, A. Umar, X. Wu, Hierarchical SnO2 nanostructures made of intermingled ultrathin nanosheets for environmental remediation, smart gas sensor, and supercapacitor applications, ACS Appl. Mater. Interfaces 6 (2014) 2174–2184, https://doi.org/10.1021/am405301v.
[56] X. Wang, X. Wang, Q. Di, H. Zhao, B. Liang, J. Yang, Mutual effects of fluorine dopant and oxygen vacancies on structural and luminescence characteristics of F doped SnO2 nanoparticles, Materials 10 (2017), https://doi.org/10.3390/ma10121398.
[57] L.Z. Liu, X.L. Wu, F. Gao, J.C. Shen, T.H. Li, P.K. Chu, Determination of surface oxygen vacancy position in SnO2 nanocrystals by Raman spectroscopy, Solid State Commun. 151 (2011) 811–814, https://doi.org/10.1016/j.ssc.2011.03.029.
[58] L.Z. Liu, T.H. Li, X.L. Wu, J.C. Shen, P.K. Chu, Identification of oxygen vacancy types from Raman spectra of SnO 2 nanocrystals, J. Raman Spectrosc. 43 (2012) 1423–1426, https://doi.org/10.1002/jrs.4078.
[59] J. Yang, S. Wang, L. Zhang, R. Dong, Z. Zhu, X. Gao, Zn2SnO4-doped SnO2 hollow spheres for phenylamine gas sensor application, Sensor. Actuator. B Chem. 239 (2017) 857–864, https://doi.org/10.1016/j.snb.2016.08.074.
[60] P.H. Suman, A.A. Felix, H.L. Tuller, J.A. Varela, M.O. Orlandi, Comparative gas sensor response of SnO2, SnO and Sn3O4 nanobelts to NO2 and potential interferents, Sensor. Actuator. B Chem. 208 (2015) 122–127, https://doi.org/10.1016/j.snb.2014.10.119.
[61] A.S.M. Iftekhar Uddin, D.-T. Phan, G.-S. Chung, Low temperature acetylene gas sensor based on Ag nanoparticles-loaded ZnO-reduced graphene oxide hybrid, Sensor. Actuator. B Chem. 207 (2015) 362–369, https://doi.org/10.1016/j.snb.2014.10.091.
[62] I.H. Kadhim, H.A. Hassan, Q.N. Abdullah, Hydrogen gas sensor based on nanocrystalline SnO2 thin film grown on bare Si substrates, Nano-Micro Lett. 8 (2016) 20–28, https://doi.org/10.1007/s40820-015-0057-1.
[63] Q. Zhang, Q. Zhou, Z. Lu, Z. Wei, L. Xu, Y. Gui, Recent advances of SnO2-based sensors for detecting fault characteristic gases extracted from power transformer oil, Front. Chem. 6 (2018) 1–7, https://doi.org/10.3389/fchem.2018.00364.
[64] P. Bechthold, M.E. Pronsato, C. Pistonesi, DFT study of CO adsorption on Pd-SnO2 (110) surfaces, Appl. Surf. Sci. 347 (2015) 291–298, https://doi.org/10.1016/j.apsusc.2015.03.149.